Preparation and Investigation of Ethylene–Vinyl Acetate Copolymer/Silicone Rubber/Clay Nanocomposites

Shoulin Fang,[1,2] Yuan Hu,[1] Lei Song,[1] Jing Wu[1]

[1]*State Key Laboratory of Fire Science, University of Science and Technology of China, Hefei, Anhui 230026, People's Republic of China*
[2]*Department of Chemistry, University of Science and Technology of China, Hefei, Anhui 230026, People's Republic of China*

Received 20 May 2007; accepted 11 October 2007
DOI 10.1002/app.30288
Published online 23 April 2009 in Wiley InterScience (www.interscience.wiley.com).

ABSTRACT: In this article, the combination of silicone rubber (SR) elastomer with synthetic iron montmorillonite (Fe-MMT) to form a kind of new flame-retardant system based on an ethylene–vinyl acetate (EVA) copolymer is first reported. Also, the flame retardancy of the EVA/SR/Fe-MMT hybrid are compared with that of EVA/SR/natural sodium montmorillonite. The structures of the nanocomposites were characterized with X-ray diffraction and transmission electron microscopy. Cone calorimeter tests and thermogravimetric analysis were used to evaluate the flame-retardant properties and thermal stability of the composites, respectively. In addition, tensile tests were carried out with a universal testing machine, and the morphology of the fracture surface was observed with environmental scanning electron microscopy. We found that SR/organophilic montmorillonite (Fe-OMT) was more effective in reducing the primary peak heat release rate of the nanocomposite, and the EVA/SR/Fe-OMT hybrid had a higher thermal stability in the deacetylated polymer than EVA/SR/sodium organophilic montmorillonite. Moreover, the exfoliated EVA/SR/Fe-OMT nanocomposite displayed excellent mechanical properties because of a better dispersion of Fe-OMT in the polymer matrix, and a possible mechanism is discussed. © 2009 Wiley Periodicals, Inc. J Appl Polym Sci 113: 1664–1670, 2009

Key words: clay; flame retardance; nanocomposites; polyolefins; silicones

INTRODUCTION

Ethylene–vinyl acetate (EVA) is a major thermoplastic polymer that is widely used in many fields, particularly in the electrical cable sheathing industry. Because of their chemical compositions, these polymers are easily flammable, and because of this, the flame retardancy of these materials has been widely studied. In flame-retardant systems of polymers, halogen-free flame-retardant additives are attracting more and more attention from researchers.[1–3] However, it is difficult to obtain a balance between flame retardancy and good mechanical properties in polymers after the addition of flame-retardant additives.

Silicon additives may be considered a universal additive for improving the fire-retardant properties of polymers and decreasing harmful impacts on environmental safety. The flame-retardant mechanism for silicon compounds is mainly a barrier layer effect.[4–6] Silicone elastomer is one silicon compound, and it has been found to improve the flame retardancy of EVA and other polymers.[7–9] Recently, polymer/layered silicate nanocomposites have been recognized as one of the most promising research fields in materials chemistry because of their unique properties.[10–14] Particularly, the labyrinth effect of the silicate layers in some polymer matrices can result in a large reduction in the peak heat release rate (HRR).[15]

In this article, iron montmorillonite (Fe-MMT) was synthesized according to the literature[16] and was organically modified by cetyltrimethyl ammonium bromide (CTAB). In this type of montmorillonite (MMT), the difference is that the Fe^{3+} ion replaces the Al^{3+} ion in the crystal lattice. Possessing a structure similar to natural MMT, this clay has similar properties to natural MMT. In addition, the incorporation of the transition-metal Fe ion within the clay interlayer is expected to enhance the fire retardancy of polymers.[17] Here, we combined silicone rubber (SR) elastomer with iron organophilic montmorillonite

Correspondence to: Y. Hu (yuanhu@ustc.edu.cn).
Contract grant sponsor: National Natural Science Foundation of China; contract grant numbers: 50476026, 50403014.
Contract grant sponsor: Specialized Research Fund for the Doctoral Program of Higher Education; contract grant number: 20040358056.
Contract grant sponsor: Program for New Century Excellent Talents in University and National 11th Five-Year Program; contract grant numbers: 2006BAK01B03, 2006BAK06B06, 2006BAK06B07.

(Fe-OMT) as a synergistic flame-retardant system based on an EVA matrix, and the flame retardancy, thermal stability, and mechanical properties were studied. Sodium organophilic montmorillonite (Na-OMT) was also used for comparison, and the corresponding nanocomposite was investigated in this study.

EXPERIMENTAL

Materials

EVA28-05, with a vinyl acetate content of 28% (density = 0.950 g/cm^3, melt flow index = 5 g/10 min), was supplied by Atofina Corp. (France). SR gel (weight-average molecular weight = 620,000, vinyl content = 0.17%) was produced by Dongjue Fine Chemicals Co., Ltd. (Nanjing, China). The vulcanizing agent, dicumyl peroxide, was provided by QiangSheng Chemical Engineering Co. (Jiangsu, China). Pristine sodium montmorillonite (Na-MMT), with a cation-exchange capacity of 96 mequiv/100 g, was kindly provided by Keyan Chemistry Co. (Hefei, China). CTAB, acidic sodium silicate ($Na_2SiO_3 \cdot 9H_2O$), iron chloride ($FeCl_3 \cdot 6H_2O$), zinc acetate [$Zn(COOCH_3)_2 \cdot 2H_2O$], and sodium hydroxide (NaOH) were all obtained from Shanghai Chemistry Co. (Shanghai, China).

Synthesis of Fe-MMT

Fe-MMT was synthesized with the following method: hydrous oxide was prepared by the mixture of $Na_2SiO_3 \cdot 9H_2O$ with $FeCl_3 \cdot 6H_2O$ and $MgCl_2 \cdot 6H_2O$ solutions to set the atomic ratio at Si : Fe : Mg = 4 : 1.7 : 0.3. The pH value (12–12.4) was adjusted with NaOH solution. Then, the slurry was sealed in a Teflon container and hydrothermally treated at 180°C for 24 h, and Fe-MMT, as a transparent yellowish brown gel, was obtained. The resulting sample was dried at 80°C for 48 h.

Preparation of organophilic montmorillonite (OMT)

The Fe-MMT and Na-MMT were dispersed in water, respectively, under vigorous stirring conditions to form a suspension. Then, a solution of CTAB was added to the suspension, and the mixture was continuously stirred for 2 h at 80°C. The suspension was centrifuged and washed with boiling distilled water to remove the excess intercalative reagent until the supernatant liquid was tested by a 0.1 mol/L $AgNO_3$ solution without yielding sedimentation. The products were then dried *in vacuo* for 48 h and ground into powders.

TABLE I
Sample Identification and Compositions

Sample	Composition
EVA	100% EVA
EVA/SR	90% EVA and 10% SR
EVA/SR/Na-OMT	90% EVA, 8% SR, and 2% Na-OMT
EVA/SR/Fe-OMT	90% EVA, 8% SR, and 2% Fe-OMT

Synthesis of the hybrids based on EVA/SR and OMT

The hybrids were prepared on a two-roll mixing mill (XK-160, JiangSu, China) at a temperature of 110°C, and the roll speed was maintained at 50 rpm. EVA was added to the mill at the beginning of the blending procedure. After EVA was molten, SR or SR/OMT was added to the matrix, and the matrix was processed until a good visual dispersion was achieved. The vulcanizing agent (1 wt %) was added last, and the resulting mixtures were then compression-molded into sheets (1 and 3 mm thick). At the same time, the sample was vulcanized at 170°C for 15 min. The samples are identified in Table I.

Characterization

X-ray diffraction (XRD) patterns were obtained with a Japan Rigaku D/Max-Ra rotating anode X-ray diffractometer equipped with a Cu Kα tube and a Ni filter (wavelength = 0.1542 nm). The range of the diffraction angle was $2\theta = 1.5$–10°.

Transmission electron microscopy (TEM) images were obtained on a Jeol (Tokyo, Japan) JEM-100SX transmission electron microscope with an acceleration voltage of 100 kV. The nanocomposite specimens were cut at low temperature with an ultramicrotome (Ultracut-1, United Kingdom) with a diamond knife from an epoxy block with the films of the nanocomposite embedded.

The flammability was characterized by a cone calorimeter. All samples ($100 \times 100 \times 3$ mm^3) were examined in a Stanton Redcroft (England) cone calorimeter according to ISO 5660 under a heat flux of 35 kW/m^2. The exhaust flow rate was 24 L/s, and the spark was continued until the sample ignited. The experiments were repeated three times, and the results were reproducible to within $\pm$10%.

Thermogravimetric analysis (TGA) experiments were performed with a Netzsch STA 409C thermoanalyzer instrument (Netzsch Company, Germany) under air flows of 50 mm/min. The specimens (ca. 10 mg) were heated from room temperature to 700°C at a linear heating rate of 10°C/min.

The tensile tests were measured on a DCS-5000 universal testing machine (Shimadzu, Japan) at room temperature and at a constant speed of 200 mm/min. All specimens were tested five times, and the values were averaged.

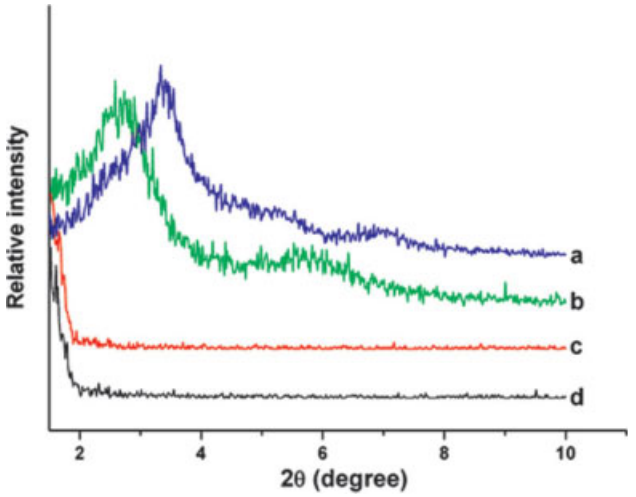

Figure 1 XRD patterns of (a) Na-OMT, (b) Fe-OMT, (c) EVA/SR/Na-OMT, and (d) EVA/SR/Fe-OMT. [Color figure can be viewed in the online issue, which is available at www.interscience.wiley.com.]

The morphologies of the fracture surface and char residue of the composites were observed and studied with environmental scanning electron microscopy (ESEM; XL 30 ESEM-TMP, Philips). All samples were coated with a gold–palladium film *in vacuo* before testing.

RESULTS AND DISCUSSION

Dispersability of the EVA/SR/OMT nanocomposites

The small-angle XRD technique was used to measure the interlayer distance of the silicate layers of the MMT and to evaluate the silicate layer distribution of organomodified MMT in the polymer matrix. Figure 1 shows the XRD patterns of the Na-OMT, Fe-OMT, EVA/SR/Na-OMT, and EVA/SR/Fe-OMT nanocomposites. The characteristic peaks corresponding to the (001) plane reflection of Na-OMT and Fe-OMT appeared at $2\theta = 3.3$ and 2.7°, corresponding to gallery spacings of 2.68 and 3.27 nm, respectively. The difference in *d*-spacing for Fe-OMT and Na-OMT may have been due to the distinction of the cation-exchange capacity of the two types of clay and the difference of arranged angle in the chain of CTAB between the silicate layers in the two kinds of clay.[18] There was no diffractive peak in the XRD patterns of the EVA/SR/Na-OMT and EVA/SR/Fe-OMT nanocomposites, which indicated that the silicate layers were exfoliated well in the nanocomposites.

TEM observation was used to prove the XRD analysis of the nanostructure. The TEM micrographs of the EVA/SR/Fe-OMT [Fig. 2(a)] and EVA/SR/Na-OMT [Fig. 2(b)] nanocomposites are shown in Figure 2. As shown in Figure 2, there were many bigger black particles, that is, SR phase, which indicated the minor SR component, as the disperse phase, was distributed within the continuum of the major EVA component. On the other hand, a lot of dark lines (clay platelets) were found in EVA. The silicate layers were homogeneously exfoliated in the EVA matrix, which agreed well with the results of the XRD analysis. Moreover, the Fe-OMT measure of dispersion in the polymer matrix was better than that of Na-OMT. Combining this with the results of XRD, we deduced that the difference occurred because the polymer chain could easily penetrate into the interlayer of clay platelets of Fe-OMT because of its larger *d*-spacing, which resulted in a less ordered stacking of clay platelets.

Flammability properties

Cone calorimeter investigations can be used as a universal approach to compare and evaluate the fire behavior of polymer materials. All materials burned homogeneously under forced flaming conditions in the cone calorimeter with a stable flame zone above the surface. HRR, especially peak HRR, has been found to be the most important parameter in evaluating fire safety.[19]

The HRR plots for the EVA, EVA/SR, EVA/SR/Na-OMT, and EVA/SR/Fe-OMT at a heat flux of 35 kW/m^2 are shown in Figure 3. During the process of combustion, each sample had two peaks HRR, which were mainly due to the two-step pyrolysis

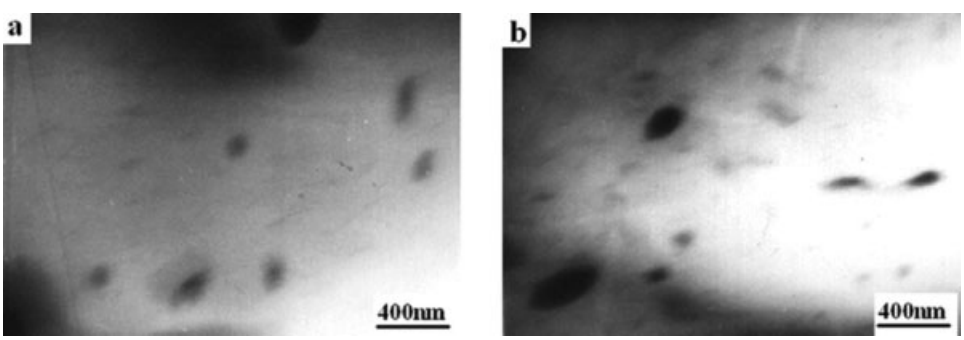

Figure 2 TEM images of (A) EVA/SR/Fe-OMT and (B) EVA/SR/Na-OMT.

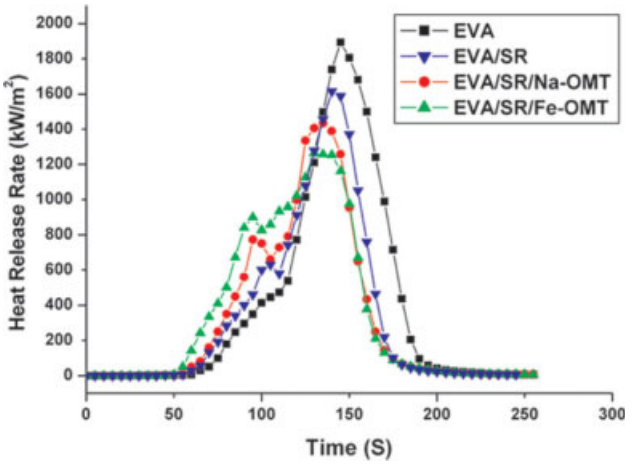

Figure 3 HRR of EVA, EVA/SR, and EVA/SR/OMT. [Color figure can be viewed in the online issue, which is available at www.interscience.wiley.com.]

behavior of the EVA composites, and the phenomenon was also proven by TGA (shown later in Fig. 5). The SR additive reduced the effective heat of combustion, and the primary peak HRR of EVA/SR was 280 kW/m^2 lower than that of pure EVA. A barrier layer mainly composed of silica was formed during the process of combustion. The peak HRR was further reduced when OMT was added to the matrix. The primary peak HRR values of the EVA/SR/Na-OMT and EVA/SR/Fe-OMT hybrids decreased by about 24.2 and 33.2%, respectively, compared with that of pure EVA. The barrier effect (in addition to the emigrated silica from SR combustion) increased because of the ablative reassembly of the reticular layers of the silicate on the surface of the polymer in the process of volatilization, and a sort of foamlike char-layered silicate material could be made.[10,20] The reassembling layers acted as a protective barrier in addition to the silica shield and could, thus, limit oxygen diffusion to the substrate and retard the volatilization of the flammable decomposition products. Therefore, more stable radicals underwent intermolecular reactions, which led to the reduction of HRR in the cone calorimeter.[21] As for the EVA/SR/Fe-OMT nanocomposite, the primary peak HRR was lower than that of the sample containing Na-OMT. Except for the previously discussed causes, the Fe ion in the structure was the operative site for radical trapping within clay, which reduced the peak HRR.[22]

However, the intensity of the subpeak HRR of the EVA/SR/Clay nanocomposites was higher than that of pure EVA at initial combustion, and the ignition time decreased in the order EVA > EVA/SR > EVA/SR/Na-OMT > EVA/SR/Fe-OMT. This may be explained by the first-step thermodegradation of EVA, which involved deacylation with the elimination of acetic acid. The elimination of the deacylation reaction was accelerated because of a catalytic effect of acidic sites of the layered silicates deriving from the Hoffman elimination reaction of the organic alkylammonium cation.[23] In nanocomposites, those acidic sites are active because of intimate contact between the polymer and the silicate. The accelerated evolution of acetic acid might have contributed to greater heat release in the early stages of nanocomposite combustion compared to the pure EVA and EVA/SR samples. At the same time, containing the transition metal, Fe-OMT revealed stronger properties of a Lewis acid (electron pair acceptor) than Na-OMT,[24] so the catalytic effect of Fe-OMT on EVA was before that of Na-OMT. Consequently, Fe-OMT was more effective in enhancing the subpeak HRR of EVA than Na-OMT, as shown in Figure 3. As for the EVA/SR sample, the reason for the higher subpeak HRR than for the pure EVA may have been that the poor compatibility of EVA and SR [shown later in Fig. 6(b,c)] destroyed the crosslink netlike structure of EVA and, therefore, accelerated the emission of volatile products.

Moreover, the flame-retardant EVA samples displayed remarkably different combustion behaviors than pure EVA during the cone calorimetry tests. At the end of combustion, pure EVA left no residue, and the EVA/SR produced only a little powder, whereas the nanocomposites, especially EVA/SR/Fe-OMT, left a solid, consistent char residue. ESEM images showed the morphology of the surface and interior of the EVA/SR/Fe-OMT nanocomposite after burning (Fig. 4). As shown in Figure 4(a), the

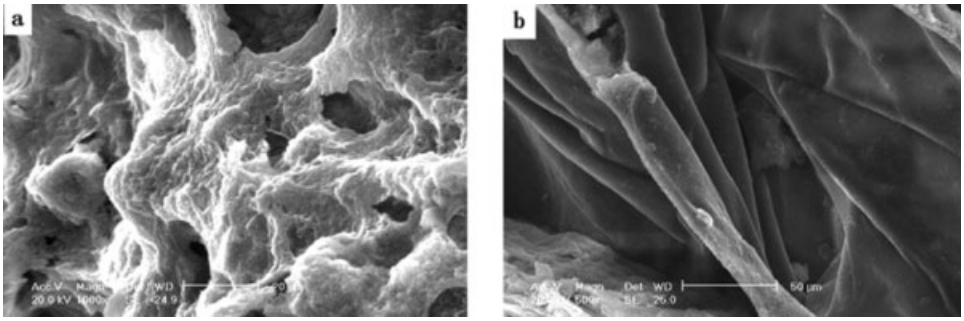

Figure 4 ESEM micrographs of (a) the surface and (b) interior of EVA/SR/Fe-OMT after burning.

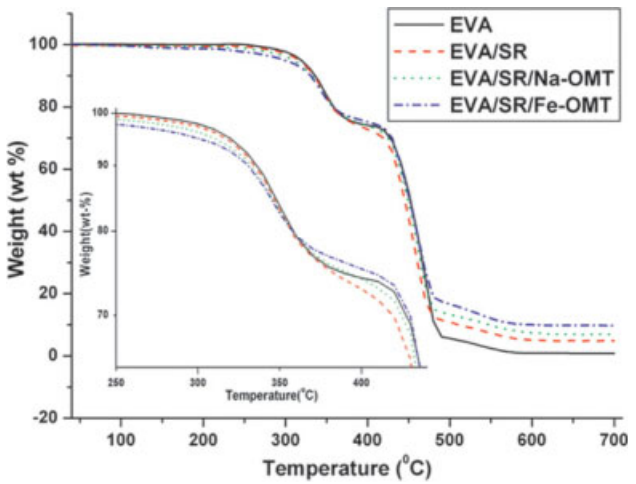

Figure 5 TGA curves of EVA, EVA/SR, and EVA/SR/OMT. [Color figure can be viewed in the online issue, which is available at www.interscience.wiley.com.]

char residue had a foamlike network barrier layer at the surface, which was similar to the results described by Maiti et al.[25] A foamlike network barrier layer can insulate the underlying material, which results in a significant reduction in the flammability. The morphology of the interior structure of the char residue revealed significant microstructural change [Fig. 4(b)], which formed a compact layer structure, which contributed to the flame-retardancy performance.

Thermal degradation stability

The thermal stability of the EVA polymer and its hybrids were analyzed by TGA, as shown in Figure 5. It is well known that EVA undergoes two degradation steps.[26,27] The first decomposition step is due to acetic acid, and the formation of double bonds occurs between 300 and 400°C with a maximum around 350°C. The second degradation step involves the aliphatic chain and leads to complete polymer volatilization. The 5% loss temperature ($T_{-5\%}$); the maximum weight-loss temperature, which includes two degradation steps (T_{max1} and T_{max2}) obtained from derivative curves; and the char residue at 700°C are listed in Table II.

The TGA data in Table II and the TGA curves in Figure 5 clearly show that the acetyl acid elimination was promoted by OMT, and $T_{-5\%}$ and T_{max1} of the EVA/SR/Fe-OMT nanocomposite were lower than those of the EVA/SR/Na-OMT nanocomposite. This indicated that the catalytic effect of the acidic sites of Fe-OMT was more evident than that of Na-OMT, which was consistent with the results of the cone calorimeter test. During the second degradation stage, the T_{max2} values of the EVA/SR and EVA/SR/clay nanocomposites showed little difference, with all being lower by about 10°C than that of pure EVA. Moreover, in the higher temperature range, the EVA/SR/Fe-OMT nanocomposite exhibited higher thermal stability, and it produced the largest char yield at 700°C. This was probably because the Fe-OMT was more advantageous for the formation of the char layer. A high-performance carbonaceous silicate char building up on the surface during thermal degradation insulated the underlying material and slowed the escape of the volatile products generated during decomposition. This result was in accord with the reduction of the HRR.

Tensile tests

The mechanical properties of EVA and its hybrids were studied by tensile tests. The results, including those of tensile strength and elongation at break, are presented in Table III. The 10% SR additive led to decreases in the ultimate tensile strength and elongation at break of the composite. This was attributed to the reduction in the crystallinity of EVA upon blending with amorphous SR. Certainly, the problem of incompatibility between the two polymers should not be ignored. Figure 6(b,c) shows the morphology of the fracture surface of EVA/SR after tensile testing. There was a clear interface between the EVA and SR phases and the existence of bigger holes in the fracture surface. Consequently, the mechanical properties of EVA/SR presented a downtrend, whereas, in the case of OMT, the nanocomposites showed better mechanical properties than the sample containing only SR. This could explained by two reasons. On the one hand, in the vulcanizing crosslinking process, OMT could have acted as active sites to increase the crosslinking degree and lead to a denser netlike structure.[28] On the other hand, the exfoliated silicate layers around the SR phase

TABLE II
Thermal Properties of EVA and EVA Composites

Sample	$T_{-5\%}$ (°C)	T_{max1} (°C)	T_{max2} (°C)	Char residue at 700°C (wt %)
EVA	319.5	350.3	469.9	0.84
EVA/SR	318.8	348.1	460.5	4.88
EVA/SR/Na-OMT	309.5	345.5	459.8	6.95
EVA/SR/Fe-OMT	300.2	339.6	459.7	9.78

TABLE III
Mechanical Properties of the EVA and EVA Composites

Sample	Tensile strength (MPa)	Elongation at break (%)
EVA	32.6	826.8
EVA/SR	27.3	772.5
EVA/SR/Na-OMT	28.6	802.9
EVA/SR/Fe-OMT	30.3	823.2

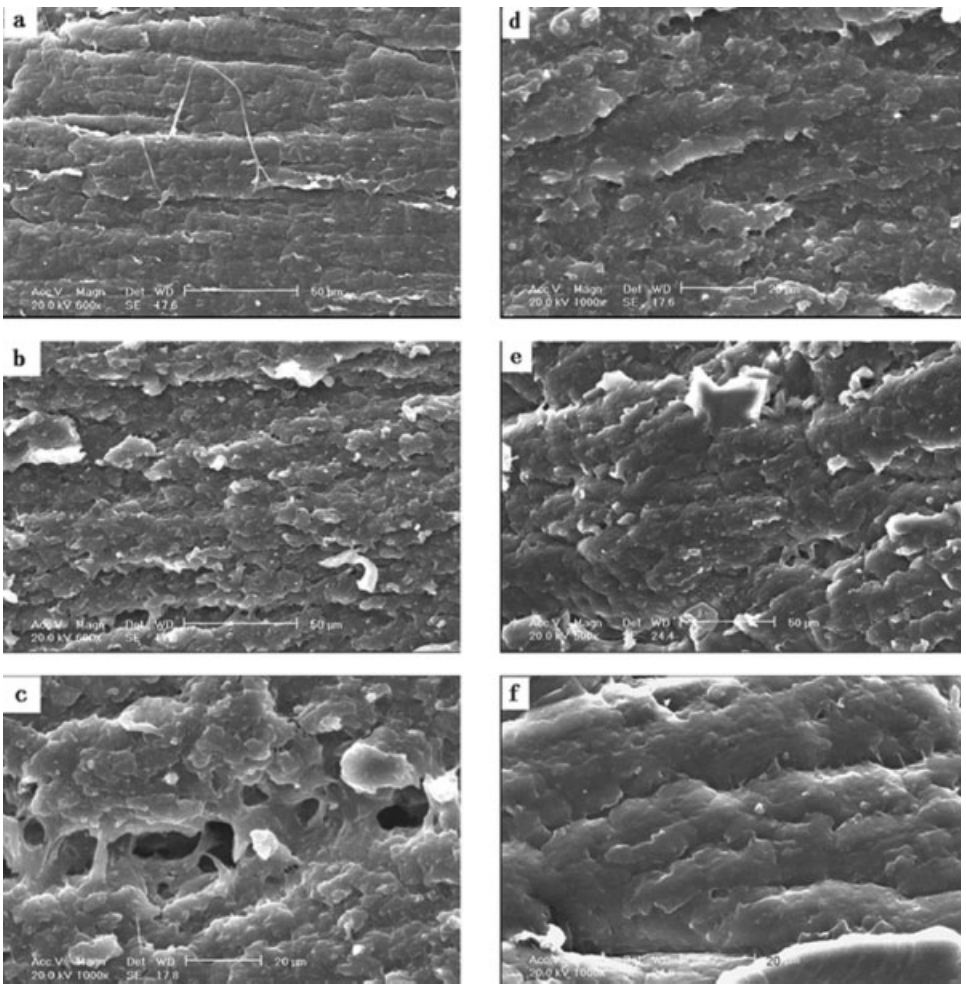

Figure 6 ESEM micrographs of the fracture surfaces of (a) EVA, (b,c) EVA/SR, (d) EVA/SR/Na-OMT, and (e,f) EVA/SR/Fe-OMT.

inhibited the coalescence of the SR domains, and at the same time, the clay platelets were difficult to aggregate because of the partitioning effect of the SR particles on the clay platelets.[29] As shown in Figure 6(d–f), after 2% OMT addition, good interfacial adhesion between the different phases of nanocomposites was observed. Moreover, because of the better dispersion of Fe-OMT in the polymer matrix, the EVA/SR/Fe-OMT nanocomposite showed higher mechanical properties than the EVA/SR/Na-OMT nanocomposite.

CONCLUSIONS

A new flame-retardant system, SR/Fe-OMT based on an EVA matrix, was first examined in this study. Experimental analyses showed that the exfoliated Fe-OMT had better dispersion in the EVA matrix than Na-OMT, and it was more effective in improving the flame retardancy, thermal stability, and mechanical properties of EVA nanocomposites. In cone calorimeter tests, the formation of a foamlike netlike barrier layer at the surface and an interior compact char layer protected the underlying material, together with the presence of radical trapping by Fe ion within clay; consequently, the primary peak HRR of EVA/SR/Fe-OMT was remarkably reduced. However, the subpeak HRR increased because of the stronger Lewis acid of Fe-OMT. TGA also showed that EVA/SR/Fe-OMT had the maximum amount of char residue at 700°C and had a higher thermal stability on the deacetylated polymer than EVA/SR/Na-OMT. From the tensile tests, we found that the addition of OMT, especially Fe-OMT, improved the tensile strength and elongation at break of the nanocomposites. On the basis of this conclusion, OMT can serve as a compatibilizer of EVA and SR. The possible mechanism is because the exfoliated silicate layers around the SR phase inhibit the coalescence of the SR domains, and better dispersions of SR particles and clay platelets are obtained.

References

1. Hornsby, P. R. Int Mater Rev 2001, 46, 199.
2. Lu, S. Y.; Hamerton, I. Prog Polym Sci 2002, 27, 1661.
3. Pal, K.; Rastogi, J. N. J Appl Polym Sci 2004, 94, 407.
4. Kashiwagi, T.; Gilman, J. W.; Butler, K. M.; Harris, R. H.; Shields, J. R.; Asano, A. Fire Mater 2000, 24, 277.
5. Ravadits, I.; Toth, A.; Marosi, G.; Marton, A.; Szep, A. Polym Degrad Stab 2001, 74, 419.
6. Mansouri, J.; Burford, R. P.; Cheng, Y. B. Mater Sci Eng A 2006, 425, 7.
7. Huang, H. H.; Tian, M.; Liu, L.; He, Z. H.; Chen, Z. Q.; Zhang, L. Q. J Appl Polym Sci 2006, 99, 3203.
8. Hermansson, A.; Hjertberg, T.; Sultan, B. A. J Appl Polym Sci 2006, 100, 2085.
9. Hermansson, A.; Hjertberg, T.; Sultan, B. A. Fire Mater 2005, 29, 407.
10. Gilman, J. W.; Jackson, C. L.; Morgan, A. B.; Harris, R.; Manias, E.; Giannelis, E. P.; Wuthenow, M.; Hilton, D.; Phillips, S. H. Chem Mater 2000, 12, 1866.
11. Wang, S. F.; Hu, Y.; Wang, Z. Z.; Tang, Y.; Chen, Z. Y.; Fan, W. C. Polym Degrad Stab 2003, 80, 157.
12. Tang, Y.; Hu, Y.; Zhang, R.; Gui, Z.; Wang, Z. Z.; Chen, Z. Y.; Fan, W. C. Polymer 2004, 45, 5317.
13. Utracki, L. A.; Sepehr, M.; Boccaleri, E. Polym Adv Technol 2007, 18, 1.
14. Mohanty, S.; Nayak, S. K. J Thermoplast Compos Mater 2007, 20, 175.
15. LeBaron, P. C.; Wang, Z.; Pinnavaia, T. J Appl Clay Sci 1999, 15, 11.
16. Nagase, T.; Iwasaki, T.; Ebina, T.; Hayashi, H.; Onodera, Y.; Dutta, N. C. Chem Lett 1999, 4, 303.
17. Weil, E. D.; Patel, N. G. Polym Degrad Stab 2003, 82, 291.
18. Lan, T.; Kaviratna, P. D.; Pinnavaia, T. J. Chem Mater 1995, 7, 2144.
19. Gilman, J. W. Appl Clay Sci 1999, 15, 31.
20. Zanteei, M.; Kashiwagi, T.; Falqui, L.; Camino, G. Chem Mater 2002, 14, 881.
21. Jang, B. N.; Costache, M.; Wilkie, C. A. Polymer 2005, 46, 10678.
22. Zhu, J.; Wilkie, C. A. Chem Mater 2001, 13, 4649.
23. Gao, Z.; Xie, W.; Hwu, J. M.; Wells, L.; Pan, W. P. J Therm Anal Calorim 2001, 64, 467.
24. Ding, Z.; Kloprogge, J. T.; Frost, R. L.; Lu, G. Q.; Zhu, H. Y. J Porous Mater 2001, 8, 273.
25. Maiti, P.; Yamada, K.; Okamoto, M.; Ueda, K.; Okamoto, K. Chem Mater 2002, 14, 4654.
26. Camino, G.; Sgobbi, R.; Zaopo, A.; Colombier, S.; Scelza, C. Fire Mater 2000, 24, 85.
27. Costache, M. C.; Jiang, D. D.; Wilkie, C. A. Polymer 2005, 46, 6947.
28. Yang, L.; Hu, Y.; Lu, H. D.; Song, L. J Appl Polym Sci 2006, 99, 3275.
29. Ray, S. S.; Pouliot, S.; Bousmina, M.; Utracki, L. A. Polymer 2004, 45, 8403.